COTS-Based Wireless Magnetic Sensor for Small Satellites

M. D. MICHELENA
I. ARRUEGO
J. M. OTER
H. GUERRERO
INTA
Universidad Poletécnica de Madrid

We report on the utilization of a commercial off-the-shelf (COTS) magnetic sensor for the mission NANOSAT-01 and the set of tests that have been developed to up-screen it. The magnetic sensor head is a Wheatstone bridge formed by four anisotropic magnetoresistances (AMR). AMR sensors are an adequate choice for medium- to high-sensitivity (~ 3 mV/V/G) and resolution (~ 3 μG) requirements, mostly due to their low weight and volume that are so interesting for the aerospace industry. The whole system installed in NANOSAT-01 is formed by two biaxial sensors with two redundant PCBs (printed circuit boards) of RAD-HARD proximity electronics, which conditions the AMR output signal, measure the temperature, and resets the AMR. This magnetic sensor belongs to the attitude control system (ACS) of the satellite.

Manuscript received January 2, 2007; revised January 2, 2008; released for publication November 13, 2008.

IEEE Log No. T-AES/46/2/936797.

Refereeing of this contribution was handled by D. Mortari.

This work was supported in part by INTA Program "I+D de Cargas Útiles," and by the Spanish Ministerio de Educación y Ciencia (MEC) under Grants NANOSAT-OWLS (ESP 2002-0382) and OPTOMAGMANTIS (ESP 2005-05278).

Authors' current address: INTA, Programas Espaciales y Ciencias del Espacio, Laboratorio de Optoelectrónica, Ctra. Ajalvir, km. 4, Torrejón de Ardoz, Madrid 28850, Spain, E-mail: (diazma@inta.es).

I. INTRODUCTION

The use of COTS (commercial off the shelf) components in space missions constitutes a plausible alternative to the use of military or rad-tolerant components. The trend of using COTS began in the 1990s and was associated most of the time with small amateur satellites [1], which succeeded if the COTS were validated in flight. In the beginning the space agencies used to be more conservative, and they avoided this emergent mean for components validation. The later reduction of budget devoted to aerospace technology was the factor that sparked off the in-flight validation of COTS.

Three main reasons support the employment of COTS in aerospace design.

1) The first reason is an economic one. The cost of the components increases linearly with the quality level guaranteed by the manufacturer. In this way rad-tolerant components are almost an order of magnitude more expensive than military components, and these are an order of magnitude more expensive than commercial components. Thus the use of COTS supposes a reduction in the cost for the component of almost two orders of magnitude.

2) The second reason is the time saving potential of COTS. The time delivery of high qualified components is very long, and when this time needs to be taken into account, the space missions result in longer schedules.

3) The last but perhaps most important reason is the continuity. Highly qualified components follow different lines of production than the commercial components. These lines for rad-hard and military components are not working continuously, but they are activated according to necessity most of the time. Instead commercial lines manufacture components in a continuous mode with very low rates of failure. This fact can have a strong influence on the degree of characterization or even on the reliability of the "highly qualified" components.

NANOSAT-01, which is a Spanish nanosatellite that was launched in December 2004, opted for in-flight validation of components in its attitude control system (ACS). In fact in-flight validation of COTS is one of the main objectives of the mission, together with the establishment of store-and-forward communications with the Spanish Earth stations that are all over the Earth's surface and with the experimentation of new technologies [2].

We describe an off-the-shelf magnetoresistive magnetic sensor, the justification of the election of this sensor, the number of tests performed on it, and its appropriate characterization for the specific mission. We conclude with the sensors integration in NANOSAT-01 and some of the in-flight measurements.

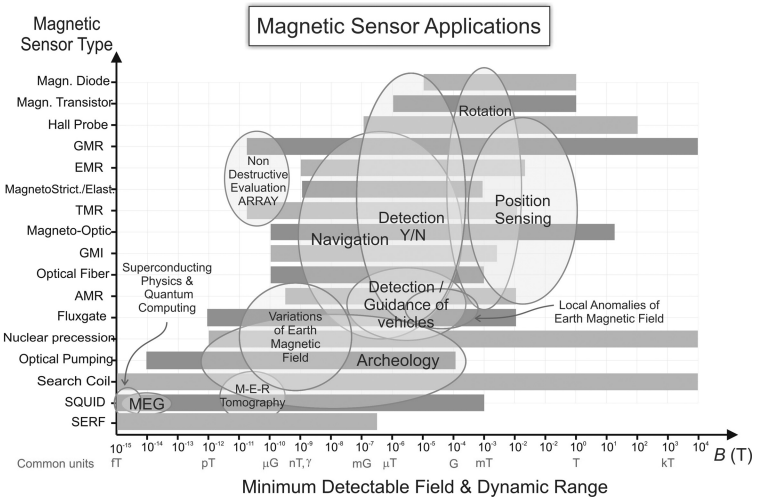

Fig. 1. Magnetic sensors versus magnetic characteristics. Ellipses represent some of application fields.

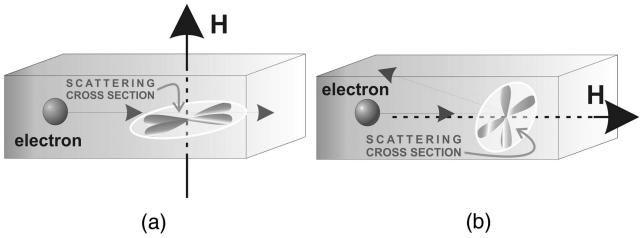

Fig. 2. AMR origin: Spin-orbit coupling.

II. AMR TECHNOLOGY

Anisotropic magnetic resistor (AMR) devices are a mature technology for magnetic field sensing. Among a great quantity of applications, these sensors cover the range of the Earth's magnetic field (0.1 mT–1 nT), which makes them a good choice for navigation (Fig. 1). In particular the use of these devices in the aerospace industry is of great interest due to their high degree of miniaturization, with a good magnetic performance to size ratio.

However this mature technology at the commercial level is not validated for aerospace use. Our goal is to validate this technology for a particular space mission: NANOSAT-01.

The AMR is basically the change of the electrical resistivity of a substance with its magnetization and thus with the magnetic field. AMR differs from ordinary magnetoresistance in that it depends on the angle between the electrical current and the magnetization of the material. The working principle of the AMR is the spin-orbit (S-O) coupling [3].

The electronic clouds of the atoms of the AMR material tend to be perpendicular to the external magnetic field, which presents a different scattering cross section for an electrical current passing through the material parallel to the magnetic field (high resistance) or perpendicular to it (low resistance) (Fig. 2).

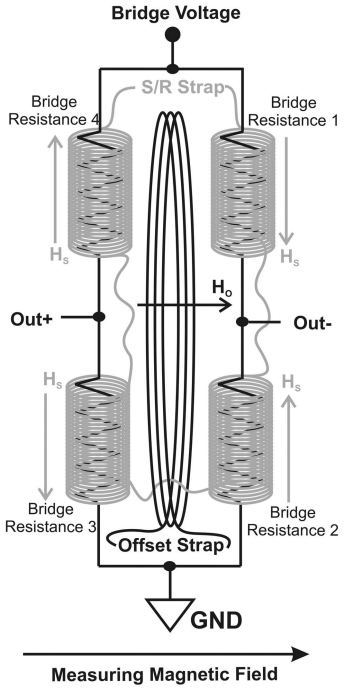

Fig. 3. Internal diagram of AMR device. Wheatstone bridge is constituted by four Permalloy stripes with easy axis perpendicular to sensing direction.

AMR devices are usually constituted by four Permalloy (or another magnetic material) stripes connected in a Wheatstone bridge (Fig. 3).

The easy axis of the Permalloy is parallel to the length of the stripe, and the stripe should be originally magnetized in the direction of the easy axis.

In the presence of a certain magnetic field applied perpendicularly to the easy axis, the magnetization of the stripes rotates, changing the magnetization state of the material and thus the electrical resistance.

The change in resistance is of the same sense in bridge resistances R1 and R3 and in the opposite sense in bridge resistances R2 and R4, which results

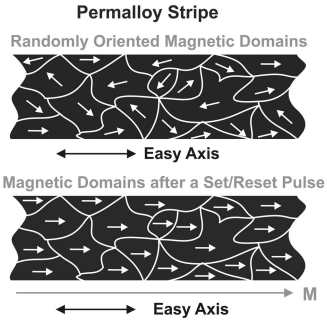

Fig. 4. Magnetization after set/reset pulse.

in an output signal four times the signal of a single stripe.

To avoid hysteresis and increase the repeatability of the sensors, the Permalloy stripe usually has a micro-coil wound to restore the initial saturation magnetization state [4]. This micro-coil is the set-reset strap in Fig. 3. When a high enough current passes through the set-rest strap, bridge resistances R1 and R3 are magnetized in one sense and R2 and R4 in the opposite sense of their easy axis.

It is the set/reset mechanism (Fig. 4) which implies that the magnetization due to the external magnetic field is a reversible procedure: by spin rotation. Each measurement is taken by starting in both magnetization senses of the same direction: SET and RESET to avoid the offset in the measurement. The intrinsic offset of the sensor can be compensated for by applying a field by means of the offset strap (Fig. 3).

The AMR sensor chosen [5] is the Honeywell HMC1021, which has an operating range of ±6 G (0.6 mT), a typical sensitivity of 1 mV/G per volt of bridge supply, and a resolution of tens of μG (10 pT). The sensor is perfectly valid for measuring the Earth's magnetic field with an accuracy of tenths of mG, which is the requirement of the ACS.

The AMR IC (integrated circuit) is an eight pin small-outline integrated circuit (SOIC) package with the surface of the chip being lower than 31 mm^2. The AMR sensor of NANOSAT-01, with the conditioning electronic, the set-reset mechanism, and the reference temperature sensing, receives the name ACS magnetic sensor (ACS MS).

III. APPLICATION IN THE ACS OF NANOSAT-01

The ACS MS, apart from being an in-orbit experiment for validating the magnetic COTS, is a part of the ACS of the satellite.

The ACS of NANOSAT-01 is very simple compared with the ACS of other small satellites [6–8] due to the fact that, in NANOSAT-01, there are no pointing requirements (solar cells are body-mounted on the quasisphere structure, antennas are omnidirectional, and no subsystem nor system requires any pointing). Therefore the ACS of NANOSAT-01 is based on four magnetic sensors and two solar sensors as sensing elements and three magnetocoils as actuators. The four magnetometers of the ACS need to be able to measure the magnetic field vector in orbit with a precision of tenths of mG (10 nT). As said before, AMR technology reaches the required resolution with acceptable values of sensitivity and of high level packing (low mass and volume but high features) in a very simple device scheme.

The AMR devices are mounted on the walls of a truncated pyramid. The measuring axis of the AMRs forms an angle of 45° with the base of the cube in such a way that the measuring axes of each sensor are not aligned with any of the main axes of the satellite. In this way, as NANOSAT-01 has a certain spin, one can extract the magnetic field vector with the measurements given by two of the sensors.

By dividing the proximity electronic of the ACS MS PCB (printed circuit board) into two parts, each of them containing two of the AMR devices, we get some redundancy in magnetic sensing. To summarize we have two biaxial magnetic sensors isolated electrically (Fig. 5), which constitute the ACS MS.

The ACS MS receives the power line from the PDU (power distribution unit) and sends six analogical signals to the OBDH (onboard data handling); four of them are of the magnetic field, and the other two are of the temperature. The ACS MS also receives a digital signal from the OBDH to reset the magnetic sensors (Fig. 6).

The head of the sensor consists of the AMR devices. The electronic conditioning of the sensor has to be designed robust enough to withstand the environmental conditions in the NANOSAT-01 orbit.

The electronic proximity consists of three blocks:

1) differential amplification of the signal proportional to the magnetic field,
2) set/reset circuitry, and
3) temperature sensing circuitry for thermal calibration.

The instrumentation amplifier has to be designed with single operational amplifiers due to some constraints of the project, which are mainly related to the availability of monolithic instrumentation amplifiers for the power supply requirements. The differential amplifier used is the OP484 due to its excellent properties in single supply. It has rail-to-rail inputs and outputs, low noise (lower than 4 nV/Hz-1/2), low offset voltage (65 μV), and high precision.

The set/reset circuitry is common for the two sensors of each part. The current that magnetizes the Permalloy stripes to saturation passes through the two microcoils in series. This design uses several capacitor discharges to provide the current pulses

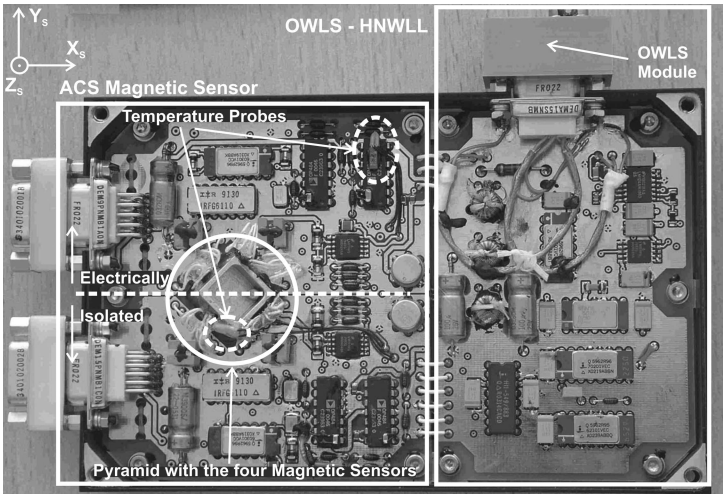

Fig. 5. ACS magnetic sensor's PCB. AMR pyramid.

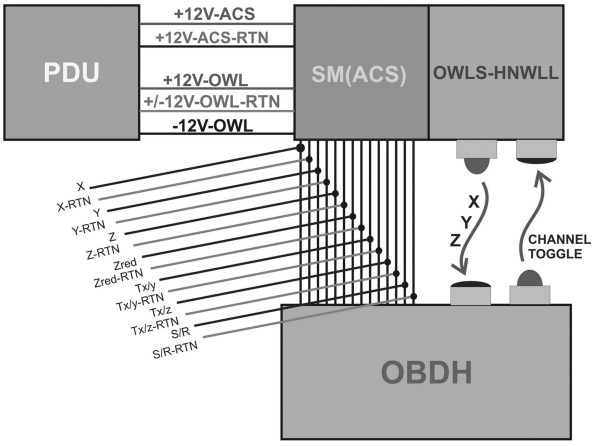

Fig. 6. Block diagram of MS (ACS) with OWLS module.

in order to avoid an excessive peak-current from the power supply.

Temperature sensing is necessary because the AMR response varies with the temperature. This variation in the operation range is linear (as specified by the manufacturer and checked in the laboratory), so it can be easily calibrated. The temperature probes are located on one AMR device and on one operational amplifier (Fig. 5).

The added value of this sensor is its capability of wireless communication with the OBDH by means of OWLS (optical wireless link for intrasatellite) communications. NANOSAT-01 aims to validate both the magnetic sensor and the OWLS channel as a complete sensor.

The redundant wireless interface is considered as a first experiment for the in-orbit qualification of this technology, and this is the reason why the link is redundant to the wired one. Data from both channels are compared on ground.

This interface makes use of near infrared (IR) light. The signals from the X, Y, and Z axes of the magnetic sensor are serialized and then converted into trains of pulses by means of a voltage-to-frequency (V/F) converter. Those pulses, whose frequency is proportional to the value of the signal, are sent to the onboard computer by means of the wireless interface. The OBDH counts them within a specific time window in such a way that the final equivalent resolution is better than 10 bits of digitalization. The computer also sends a pulse in a different IR wavelength to command the change of the axis to be read. Each time one of these pulses is received by the sensor unit, the selected channel at the input of the V/F converter is changed. A fourth channel with a reference voltage is added so that the knowledge about what channel is being received can be recovered if it is lost for any reason.

All the optoelectronic components used in this experiment are COTS that have been previously tested under total dose and protons [9]. The rest of the components are rad hard.

The resulting PCB (Fig. 5) has the two redundant biaxial magnetic sensors, their respective conditioning electronics, and the OWLS link (OWLS-HNWLL), with its OWLS module (photodiode and LED) in the wall of the box. It can be seen that the OWLS module has been adapted to a conventional DB-9 connector.

In this paper we focus on the ACS MS and not on the OWLS link [10].

IV. TESTING

Functionally this kind of sensor is an appropriate candidate for measuring the Earth's magnetic field in a low Earth orbit (LEO). But in the beginning of the project, the technology readiness level (TRL) of the AMR commercial sensors was only 7. That is the reason for the development of a number of tests to qualify the COTS for a concrete aerospace mission.

The tests developed for the sensor can be classified into two groups:

1) on the one hand the up-screening tests,

2) on the other hand the radiation tests, both devoted to up-qualify the COTS.

The following sections describe the tests developed for the subsystem or unit containing the ACS MS or for the AMR itself and the corresponding results.

A. Up-Screening

Up-screening is comprised of the following tests performed by the AMR sensor: vibration, outgassing, and temperature-aging.

The first two tests were performed at INTA resources, while the last one was performed with the INTA specifications at TECNOLOGICA.

1) *Vibration Test*: The requirements for vibration are those imposed by the launcher, ARIANE 5. In NANOSAT-01 the vibration was performed at subsystem level (NST/INT/V10/PRO/-10 issue 1). That is, the subsystem composed by the solar sensor, the magnetic nanosensor, the two OWLS experiments of NANOSAT-01, and the ACS MS.

The previous requirements for the tests are those specified in the European Cooperation for Space Standardization norm ECSS-E-10-03A.

Regarding the mechanical requirements a tightening torque of 7.5 Nm $\pm$ 10% is specified for the M6 screws and a tightening torque of 25 Nm $\pm$ 10% for M8 screws.

The environmental conditions are a temperature of 22°C $\pm$ 5% and a relative humidity (RH) of 50% $\pm$ 10%.

The tolerances for the vibration test are:

1) in acceleration: $\pm$10%,
2) in the PSD: $\pm$1.5 dB from 20 to 500 Hz and $\pm$3 dB from 500 to 2000 Hz,
3) in frequency: 1% up to 500 Hz and $\pm$2% for higher frequencies, and
4) in the duration: $\pm$5 s.

The philosophy of the test is composed of three main steps for each axis:

1) A low level sine sweep to test the integrity of the unit under test (UUT) and to find the resonance.
2) The sweeping velocity is 2 Oct/min with a starting value of 0.5 g.
3) The duration of this sine sweep is 30 s.

A high level sine sweep with the profiles of Fig. 7(a) and (b) for the vertical and horizontal axis, respectively. This sweep has a velocity of 2 Oct/min. For the vertical axis from 5 to 9 Hz, a displacement of 25 mm p-p is applied, while from 9 to 100 Hz, the UUT experiences an acceleration of 3.75 g. The profile for the horizontal axes is of the same shape with different values (Fig. 7(b)). The test succeeds if, after a visual inspection, there is no visible damage, the functionality of the UUT is demonstrated, and it withstands another low sine sweep with on effects.

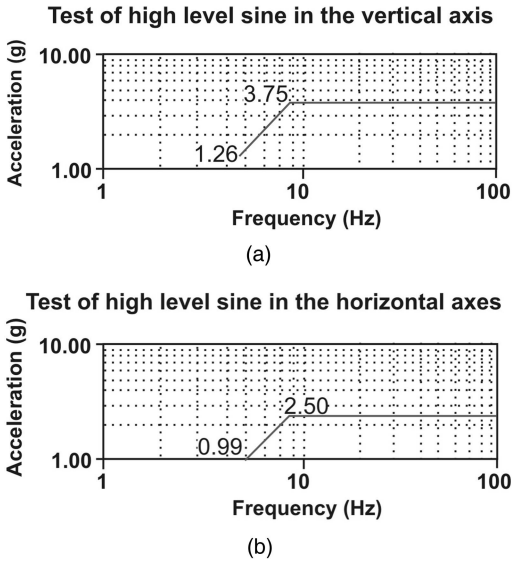

Fig. 7. Profile of sine sweep in vertical (a) and horizontal (b) axes.

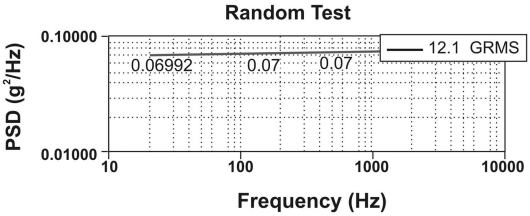

Fig. 8. Profile of random test.

A random test: the duration of this test is 120 s. In this case a plane profile of 0.0727 g^2/Hz is applied between 20 and 2000 Hz (Fig. 8).

2) *Outgassing Test*: The outgassing test is performed at the IC level, and its objective is to test the air tightness of the package. This is a necessary procedure mostly when there are visible irregularities in the package.

To develop the outgassing test, a representative quantity of devices is needed, so 20 devices are used. The ICs have their pins cut so as not to increase the mass of the testing material with metallic parts. The outgassing test was developed at INTA resources according to the European Space Agency specification ECSS-Q-70-02A.

The test consists of the measurement of the sample weight in the same environmental conditions before and after decreasing the ambient pressure.

The samples are maintained at a temperature of 20°C $\pm$ 1°C and at 65% $\pm$ 5% RH during the 24 hr before the experiment to control the adsorption of humidity.

During the test, the pressure is decreased up to 10^{-7} Torr in the position of the samples.

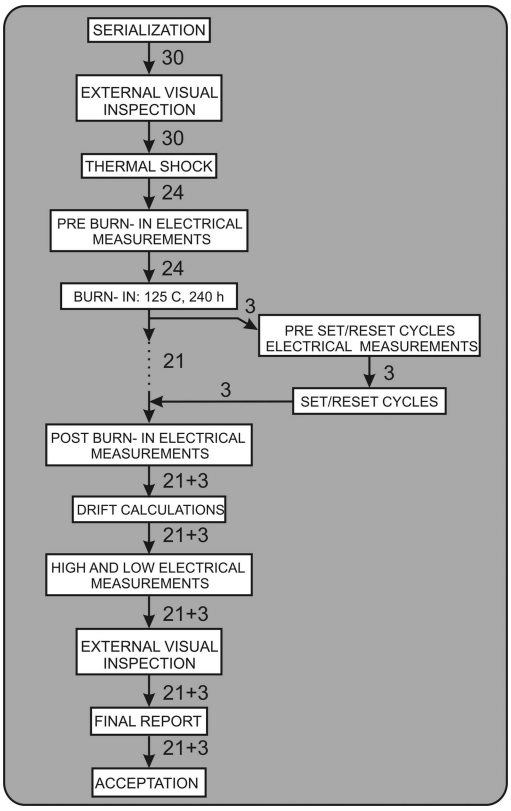

Fig. 9. Test flow block diagram.

The postconditioning is the same as the preconditioning: 24 hr at 20°C ± 1°C and at 65% ± 5% (RH).

The result is successful. The weight remains constant before and after the process.

3) *Temperature-Aging*: This process is the sequence of tests developed for a representative quantity of AMRs (IC level) of a batch to measure its level of reliability and the possible temporal drifts of the components. The temperature-aging (TA) process is undertaken for 30 units of a batch of 100 units of Honeywell HMC1021-S. The tests are focused on the resistance of components to changes in temperature, tolerance to the extreme temperatures, and aging. In addition the variation of the AMRs magnetic response, the electrical characteristics with the temperature in the operation range of NANOSAT-01, and the drifts after an aging process equivalent to that of NANOSAT-01 are measured.

Fig. 9 shows the block diagram of the up-screening process.

The first step of the process is a serialization of the 30 components in order to identify them unambiguously. Each component is marked with the part, batch, serial, and the identification numbers.

The components already serialized are visually inspected following the norm MIL-SDT-883 method: 2009, which is the criterion of acceptance/rejection of the components specified in the norm and in the JESD22-B101 document (JEDEC Standard).

The TA test begins with a thermal shock under the MIL-SDT-883 method: 1011, B test condition. The acceptance/rejection criterion is the one specified in the norm.

From now on the test continues with just 24 components of the batch. The other 6 are put aside as spares of the 24 under test, which may need to be replaced in case of failure.

To measure the drifts there is an initial characterization of the components in which all the electrical properties of interest are measured [5].

1) Bridge Resistance (without field)
2) Bridge offset (in the presence and in the absence of magnetic field). This magnitude is measured for seven different values of magnetic field: ±1.5 G, ±1 G, ±0.5 G, and 0 G.
3) Electrical resistance of the offset strap (without field)
4) Electrical resistance of the set/reset strap (without field)
5) Sensitivity (mV/Oe) when applying a ramp of magnetic field (from −1.5 G up to +1.5 G).

These are the properties measured everytime so that a characterization is performed throughout the entire process.

The acceptance/rejection criterion is the maximum and minimum levels specified in the datasheet [5]. If any of the components is out of range in one or more of the parameters, it is substituted by one of the 6 remaining serialized components.

As the response of the components in the presence of a magnetic field is a function of the position, each component is associated with a determined socket in a PCB (Fig. 10) where the field has been spatially characterized as a function of the current passing through the wires of the solenoid. The sockets used are special sockets for tests and burn-in made by 3M. The magnetic elements of the socket are substituted by nonmagnetic elements so as not to distort measurements with field.

The thermal shock is followed by an electrical characterization; the 24 components undergo a burn-in test in which the temperature is raised to 125°C during 240 hr (without magnetic field). After this to check the behaviour, 3 of the 24 components are subjected to 1.410.000 set/reset cycles between −20°C and +75°C (Fig. 7). The electrical parameters are measured again in the 24 components tested before and after the set/reset cycling: the 21 that did not undergo the cycling test and the 3 that experienced the set/reset cycling. In the block diagram this is indicated by 21 + 3 to clarify that 3 components of the total underwent the set/reset cycling. These measurements permit us to calculate the possible drifts of the tested components.

The last step consists of the measurement of the electrical properties at the maximum and minimum

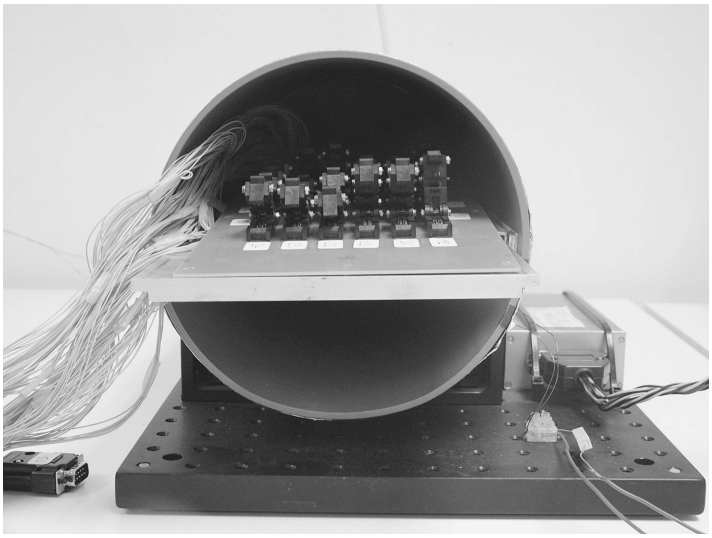

Fig. 10. Test bench for AMR devices.

temperatures expected in NANOSAT-01 (+75°C and −20°C).

The components tested are visually inspected after the tests under the norm MIL-SDT-883 method 2009, which is the acceptance/rejection criterion, the one specified in the norm and the information contained in the JESD22-B101 (JEDEC Standard).

Although the results of the tests are satisfactory, there are two kinds of variations in the measured parameters: the ones due to changes in temperature (which can be characterized) and the time variations, i.e., drifts. These two deviations are explained in the following sections.

a) *Thermal variations*: The variations in temperature are studied in order to choose devices whose Wheatstone bridge remains balanced at the zero field independently of the temperature and in order to reject the devices that do not comply with the values of the specified range in the datasheet [5]. The bridge resistance of the IC is nominally 1100 Ω, varying from 800 to 1300 Ω, according to the datasheet of the manufacturer. The variation in temperature in the range from −40 up to 125°C is approximately 2.5 Ω/°C. However the separate variation with temperature of the individual resistors in the Wheatstone bridge is not specified.

In the studied sample there is no device out of range in the range of temperatures from −20°C up to +75°C, but most of the devices become unbalanced with changes in temperature; that is, the variation of the four AMRs' straps of the bridge is not the same in the same increment of temperature. To choose the most appropriate components, the cross products (R1*R3 and R2*R4 in Fig. 3) of the values of the magnetoresistors are checked at the maximum and minimum temperatures. Among the 30 ICs tested, we show only the results of the four best devices, which are chosen for the FM ACS MS of NANOSAT-01, though the explanation is extended to all the devices tested. Table I lists the characteristics of the frequency modulation (FM) devices. Note that the environmental magnetic field is monitored during the test and that is variations are also listed in the table. It can be seen, as was expected, that the value of the resistors increases when the temperature increases, with a maximum increment of 21.6% in the full range (95°C). This fact implies a decrease in sensitivity when the temperature increases (up to 30% full scale (FS)) because relative changes in the resistance are lower. The changes in the offset strap are characterized to recognize the compensating field that is applied at each temperature. In NANOSAT-01 the offset of the sensors is characterized for each temperature, and no correction is done with the offset strap. This is possible because, even in the worst case for the FM ICs (the device N. 22 with the highest offset), the signal-to-noise ratio in the available range is enough for the mission.

The change in the set/reset strap is not a problem either. The necessary current to create the field that resets the AMRs is calculated for the highest value of the resistor (when the temperature is high), and then the corresponding current in the cold case is checked to make sure it does not exceed the specified values.

Finally the variations of offset are very low. Table I lists the changes in the offset and in the H_x and H_y components of the magnetic field measured by the sensors. The variations are taken respective to the values of the magnetic field components at 25°C: H_x = 51 mOe, and H_y = 183 mOe.

Studying the response of the sensors and the magnetic field vector in their position, it can be seen that the variations of the offset are mostly due to the changes in the magnetic field.

Besides it can also be seen that devices N.: 4, 21, and 22 have more influence from the component

TABLE I
Thermal Variations

Device	Temperature (°C)	ΔH_x (mOe)	ΔH_y (mOe)	Bridge Resistances R_1 (Ω)	R_2 (Ω)	R_3 (Ω)	R_4 (Ω)	Offset Strap (Ω)	Set/Reset Strap (Ω)	Sensitivity (mV/Oe)	Offset (mV)
	−20	−5	68	994	994	994	994	35.63	7.11	4.91	−0.16
4	25	0	0	1076	1076	1080	1078	43.16	8.5	4.42	−0.49
	75	−12	95	1120	1120	1122	1122	50.6	8.99	3.85	−0.36
	−20	−5	68	908	908	908	908	36.28	5.63	4.88	0.26
16	25	0	0	992	994	998	1000	43.89	6.81	4.32	0.48
	75	−12	95	1094	1094	1098	1098	51.42	8.01	3.59	0.83
	−20	−5	68	900	900	902	902	35.8	5.66	4.92	−0.57
21	25	0	0	996	996	1004	1002	43.39	6.84	4.34	−0.64
	75	−12	95	1108	1110	1110	1114	50.76	8.02	3.61	−0.35
	−20	−5	68	944	944	946	946	35.74	6.77	4.93	−1.38
22	25	0	0	1046	1046	1052	1050	43.28	8.2	4.34	−1.5
	75	−12	95	1170	1170	1174	1174	50.71	8.63	3.62	−1.19

TABLE II
Drifts Due to the Burn-In Test

Device	ΔH_x (mOe)	ΔH_y (mOe)	ΔR_1 (%)	ΔR_2 (%)	ΔR_3 (%)	ΔR_4 (%)	ΔOffset Strap (%)	ΔSet/Reset Strap (%)	ΔSensitivity (%)	ΔOffset (%)
4	−8	10	−1.49	−1.3	−1.67	−1.48	−1.41	−1.41	0.05	12.58
16	−8	10	−1.01	−1.01	−1	−1.2	−1.34	−1.17	0.05	−29.56
21	−8	10	−1	−1	−1.39	−1.2	−1.43	−1.32	0.05	9.37
22	−8	10	−0.96	−0.96	−1.52	−0.95	−1.32	−1.22	0.48	0.27

of the field in the X direction, while the N. 16 experiences a stronger influence from the magnetic field in the Y direction. That is, their orientation is not exactly the same.

All these changes are temperature-dependent variations, and thus we do not suppose them to be permanent variations, but the original values reestablish themselves once the initial temperature is reached. Thus the behaviour of the sensors with the temperature can be characterized.

b) *Drifts*: Again there are two different kinds of drifts: the ones due to the burn-in process and the ones due to the set/reset cycling.

Drifts due to the burn-in test: The electrical parameters and the magnetic response are measured before and after the burn-in test. Again there is a certain variation of the environmental magnetic field between the measurements (an absolute change of −8 mG or a −16% in the X component and 10 mG or a 5% in the Y component). This causes a variation of the offset (higher in component N 16 and more affected by the variation of the Y component of the field), and a change in the magnetoresistors that can be estimated (Table II).

But there are other drifts in the values that are not associated with changes of the magnetic field. These changes occurr as a consequence of the burn-in test, and they are fairly homogeneous in the sampling. The variation of the resistors is always the same, this is, decreasing the resistors' values, and the variation is lower than 2%, except for one magnetoresistor of the device N. 14 (not chosen for any of the models).

The change in sensitivity is lower than 1%, except for three devices not chosen for any of the models (N. 8 with 1.08%, N. 18 with 1.66%, and N. 20 with 1.16%). In the chosen devices the maximum change in sensitivity is 5%. This is perfectly acceptable because, although an error of 1 mG is supposed when the absolute value of the magnetic field is 1 G, the relative measurements are not affected by this error.

The drift of the offset and set/reset straps is lower than 2.5%.

Again these drifts are acceptable. On one hand a drift in the offset of the 2.5% supposes a displacement of the measuring field of 2.875 mG for every field, and thus the relative changes in the field are not affected by the drift. In any case the existing offsets are low enough so as not to employ the offset strap but characterize the offset. On the other hand the change of the set/reset strap just supposes a maximum change in the current pulses of ±20 mA added to the 1 A nominal pulses, which is enough to reset the sensor, as the range of necessary pulses is from 0.5 A up to 4 A.

To summarize the burn-in test is satisfactory. Twenty-four of the samples are accepted.

Drifts due to the set/reset cycling: The set/reset cycling is somehow an aging of the components. In this test the components are subject to the number

TABLE III
Set/Reset Cycling

Device	R_1 (%)	R_2 (%)	R_3 (%)	R_4 (%)	Offset Strap (%)	Set/Reset Strap (%)	Sensitivity (%)
1	−0.4	−0.4	−0.4	−0.6	−0.4	−0.4	0
2	−0.6	−0.4	−0.4	0	−0.4	−0.5	−0.1
3	−0.8	−0.4	0	−0.2	−0.2	0.9	0.1

TABLE IV
Post-Irradiation
HMC1001 Electrical Measurements

Device	Dose Rate (krad/h)	Total Dose (krad)	R_1 (Ω)	R_2 (Ω)	R_3 (Ω)	R_4 (Ω)	Offset Strap (Ω)	Set/Reset Strap (Ω)
1	0.378	33.6	877.8	877.5	878	877.7	2.28	1.66
2	3.18	282.3	868	871.5	870.3	869.2	2.34	1.63

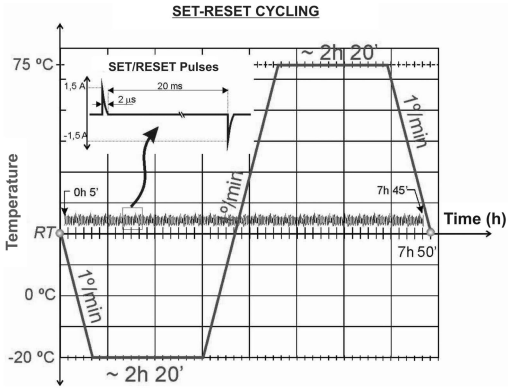

Fig. 11. Temperature profile of set/reset cycling.

of set and reset current pulses that correspond to the number of pulses (but at higher frequency) in a three year mission at the extreme temperatures of operation (Fig. 11) This cycling is performed just in three components of the sample because it is considered to be stressful for the components.

The result of the cycling is also successful (Table III). The magnetic field during this test is quasiconstant.

The drift of the magnetoresistors does not reach in any case 1%, the mean value of the drift being 0.37%.

The change in sensitivity is lower than the 0.1%, but again this doesn't affect the relative measurements, but it does affect the absolute ones.

It happens the same with the offset and set/reset straps, whose variation after the cycling is lower than 1%.

To summarize it can be said that the AMR devices are suitable for the measurement of the magnetic field of the Earth in the LEO of NANOSAT-01 during the three year mission.

B. Radiation Tests

Although we assume that AMR technology is immune against radiation, we have developed some irradiation tests: irradiation with γ-rays and irradiation with protons at levels equal or higher of those expected in NANOSAT-01.

1) *γ-Ray Irradiation Test (TID—total ionizing dose)*: The first test was developed in the CIEMAT Gamma Irradiation facility in Madrid. This facility consists of a steel cylinder immersed in a pool with ^{60}Co sources at the bottom. This configuration, with water instead of open-air, permits good control of the total dose and the rate of irradiation. Besides to obtain different doses for the different devices under test (DUT), a mobile bench was designed, in which a lead shielding was provided for each set of components.

In the first irradiation campaign developed in these facilities, two Honeywell (HMC1001) AMR monoaxial magnetic sensors were irradiated. The HMC1001 was the device originally chosen for the mission, which had the same technology as the HMC1021 finally used. In this test the electrical measurements that were performed after the tests showed that both devices passed the test and that all the electrical parameters were in the datasheet-specified range (Table IV).

The second irradiation campaign was devoted to irradiate the HMC1021, which was the component finally used in the ACS magnetic sensor. The dose rate during the irradiation was not constant, but instead it varied from 0.5 rad/h up to 50 rad/h. The electrical parameters were measured in the same conditions before and after the tests. The drifts for a total dose of 4.66 krad in the AMRs were lower than 4%, the ones of the offset strap were lower than 7%, and those of the set/reset strap resistance were of the order of 5%. All the resistors of the bridge decreased after the irradiation with γ-rays. These drifts were acceptable. In terms of the magnetic field, the drift supposed a change of field of 33 mG at the half life of the mission (assuming that the irradiation in space would be homogeneous during the mission). As all of the AMRs decrease at almost the same rate, the Wheatstone bridge remained balanced. The increase in sensitivity due to the decrease of the value

TABLE V
Post-Irradiation
HMC1021 Electrical Measurements

	Bridge Resistances					
Total Dose (krad)	R_1 (Ω)	R_2 (Ω)	R_3 (Ω)	R_4 (Ω)	Offset Strap (Ω)	Set/Reset Strap (Ω)
0	756.8	757.23	758.62	758.45	43.39	7.27
4.65	754.5	753.97	755.99	755.82	43.1	6.9

of the AMRs was also acceptable. The drift of the offset strap did not involve any change because in NANOSAT-01 this compensation was not employed. Regarding the set/reset strap, the decrease of the resistance implied an increase of 5% in the current passing through the strap, which did not exceed the allowed range, but obviously it saturates the magnetoresistances (Table V).

2) *Protons Irradiation Test (Displacement Damage)*: The reason to irradiate with protons instead of particles was that the rest of the components irradiated, apart from the AMR, were optoelectronic components mostly susceptible against protons. The proton tests were developed at the Cyclotron Research Center (CR) of the Catholic University of Louvain-la-Neuve (UCL). The irradiation was done in six steps [9] by using 52 MeV protons, with a flux of 2.5 10^8 protons/cm^{2}s (Table VI). The beam diameter was 10 cm so that the irradiation was homogeneous all over the AMR device located at the top of the PCB (Fig. 12), in a specific socket where all magnetic parts were removed and changed to brass ones.

In this test just two of all the electrical parameters specified in the datasheet were measured: the electrical resistance of the set/reset strap and that of the offset strap. No measurement of the resistance of the bridge was performed. Instead we measured the Wheatstone bridge output voltage in the presence of a magnetic field, which was completely equivalent but has some physical sense. Besides a great dispersion of the resistance has ben observed of the AMRs of the bridge, sometimes even exceeding the specified values in the datasheet despite correct functioning of the device.

As happens with γ-rays irradiation, the value of the resistors decreased. In this case the change in the value of the set/reset strap was approximately 8%. Anyway the change in current due to this decrease in the value of the resistance of the strap was acceptable.

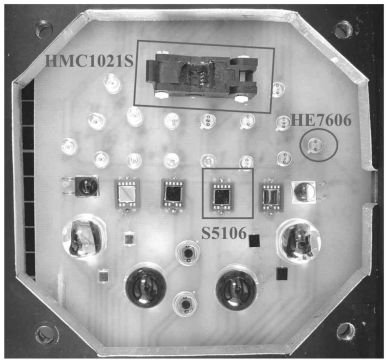

Fig. 12. Array of devices to be irradiated with protons. As can be seen at top of picture, the metallic parts of the AMR socket and substituted by nonmagnetic ones. Optoelectronic components used in OWLS link were also irradiated: photodiode S5106 by Hamamatsu and IRED HE7606 by Hitachi.

The offset produced by the irradiation was equivalent to 8 mG, and thus it was not a high drift. The changes in sensitivity were 2%, which were higher than those obtained with the other tests but were still acceptable as a drift of the 2% in the sensitivity meant an error of 1.67 mG in the absolute value of the magnetic field.

V. ON EARTH CHARACTERIZATION

The ACS MS was characterized on Earth to provide the ACS the magnetic field in which the satellite was to be immersed. The characterization was developed in the following steps.

1) Temperature characterization of the sensor response with the magnetic field at PCB level.
2) Characterization of the sensor response with the magnetic field once the satellite is fully integrated.

The first step of the characterization was developed at the INTA environmental chambers. Fig. 13 shows the equipment test for the rough measurements: the PCB in the center of a pair of Helmholtz coils in an environmental chamber. For better accuracy of measurement, a set of a triaxial system of Helmholtz coils and the ACS MS were put into a zero field chamber, and all of this equipment was put into a room-sized environmental chamber. These measurements resulted in a set of curves for each of

TABLE VI
Post-Irradiation Variation of the Response

Flux (10^8 p/cm^{2}s)	Fluence (10^{10} p/cm^2)	ΔV (mV)@ $H = -1Oe$	ΔV (mV)@ $H = 0Oe$	ΔV (mV)@ $H = 1Oe$	Offset Strap (Ω)	Set/Reset Strap (Ω)
0	0	−9.5	3.1	15.7	45.214	7.491
2.5	208.4	−9.7	3.2	16.1	42.742	6.898
Specified* Min, Typ, Max		−15 −12 −9.6	−10 ±2.5 11.25	9.6 12 15	38 50 60	5.5 7.7 9

Fig. 13. Temperature characterization of MS with magnetic field created by pair of Helmholtz coils in environmental chamber.

Fig. 14. Characterization of ACS MS in Earth magnetic field simulator.

the four AMR sensors: the response of each sensor with the three orthogonal components of the magnetic field for a number of temperatures.

The second characterization had to include the deviation of the previous curves due to the integration of the ACS MS in the satellite and the contribution to the MS response of the magnetic elements of the satellite.

This characterization was developed at a controlled temperature in INTAs Earth field simulator of INTA (Fig. 14).

In the Earth field simulator, a magnetic field characterization of the sensor integrated in the satellite at a fixed temperature was performed. The final equations to solve the Earth magnetic field components in function of the sensors response and the temperature were obtained by matching the results of the temperature measurements of step one with the measurements of step two.

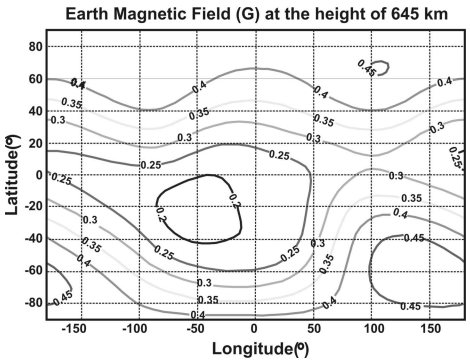

Fig. 15. Magnetic field in NANOSAT-01 orbit.

TABLE VII
Experimental Parameters for (1)

Sensor	Field Component	A Value	B Value
X	X	$A_x^{\text{Sensor } X} = 0.1087T_{xz} - 3.7219$	$B_x^{\text{Sensor } X} = 0.01$
	Y	$A_Y^{\text{Sensor } X} = 0.0813T_{xz} - 2.7467$	$B_Y^{\text{Sensor } X} = 0.01$
	Z	$A_Z^{\text{Sensor } X} = -0.076T_{xz} + 2.5977$	$B_Z^{\text{Sensor } X} = 0.01$
Z	X	$A_x^{\text{Sensor } Z} = 0.0905T_{xz} - 3.257$	$B_x^{\text{Sensor } Z} = 0.6997 - 0.03183T_{xz}$
	Y	$A_Y^{\text{Sensor } Z} = -0.0733T_{xz} + 2.584$	$B_Y^{\text{Sensor } Z} = 0.6997 - 0.03183T_{xz}$
	Z	$A_Z^{\text{Sensor } Z} = -0.0705T_{xz} + 2.3604$	$B_Z^{\text{Sensor } Z} = 0.6997 - 0.03183T_{xz}$
Y	X	$A_x^{\text{Sensor } Y} = -0.0448T_{yz} + 1.530$	$B_x^{\text{Sensor } Y} = -0.0993 + 0.0054T_{yz}$
	Y	$A_Y^{\text{Sensor } Y} = 0.0817T_{yz} - 2.741$	$B_Y^{\text{Sensor } Y} = -0.0993 + 0.0054T_{yz}$
	Z	$A_Z^{\text{Sensor } Y} = -0.1268T_{yz} + 4.458$	$B_Z^{\text{Sensor } Y} = -0.0993 + 0.0054T_{yz}$
Zred	X	$A_x^{\text{Sensor } Z_{\text{red}}} = 0.0212T_{yz} - 1.432$	$B_x^{\text{Sensor } Z_{\text{red}}} = -0.0177 + 0.00065T_{yz}$
	Y	$A_Y^{\text{Sensor } Z_{\text{red}}} = 0.0592T_{yz} - 2.652$	$B_Y^{\text{Sensor } Z_{\text{red}}} = -0.0177 + 0.00065T_{yz}$
	Z	$A_Z^{\text{Sensor } Z_{\text{red}}} = 0.1072T_{yz} - 4.345$	$B_Z^{\text{Sensor } Z_{\text{red}}} = -0.0177 + 0.00065T_{yz}$

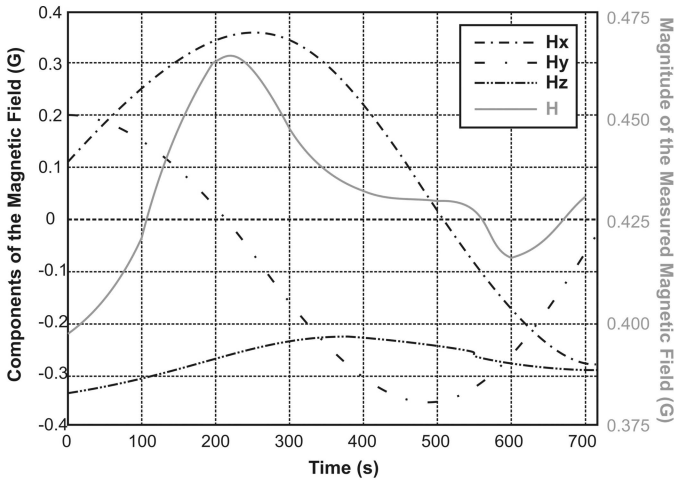

(a)

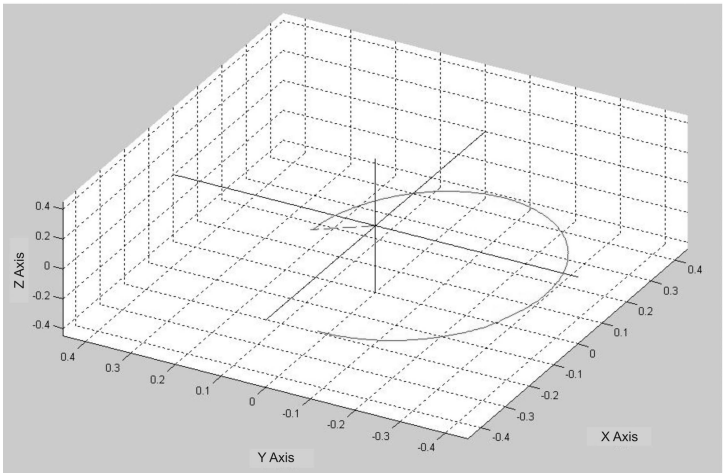

(b)

Fig. 16. Components of magnetic field in one of first activations ACS MS with modulus of magnetic field (a). Rotation of magnetic field vector from point of view of satellite (b).

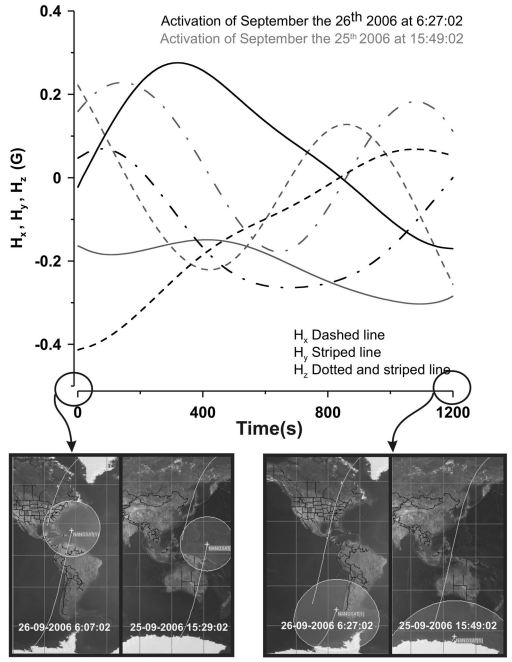

Fig. 17. Components of magnetic field in two activations of September 2006: 25th at 15:49:02 UTC and 26th at 6:07:02 UTC. Position of NANOSAT-01 in starting and ending points of activations.

The equation for the sensor "i" is the following:

$$V^{\text{Sensor}_i}(V) = [A_X^{\text{Sensor}_i} H_X + B_X^{\text{Sensor}_i}] + [A_Y^{\text{Sensor}_i} H_Y + B_Y^{\text{Sensor}_i}] + [A_Z^{\text{Sensor}_i} H_Z + B_Z^{\text{Sensor}_i}] \quad (1)$$

where coefficients A and offsets B are temperature dependent (Table VII).

Note that, in Table VII, the coefficients and the offset of the sensors are related to the temperature measurement of their PCB, but the caracterization is made with both temperature measurements so that one temperature sensor can fail.

The data provided to the ACS are the four equations corresponding to the four magnetic sensors, with the temperature-dependent values of the parameters A and B.

VI. IN ORBIT RESULTS

NANOSAT-01 was launched December 18, 2004 in the ASAP of ARIANE 5 from French Guiana. With a quasi-polar LEO, NANOSAT-01 was born to store and forward communications with Earth stations in remote locations.

The first data of the ACS magnetic sensor measured Earth's magnetic field in orbit (Fig. 15), and thus by adding the data from the solar sensors, the attitude of the satellite was derived.

As it has been explained, although the sensor is used by ACS, it is also considered an experimental sensor to be validated in orbit. In this sense some activations are being programmed to generate raw data from it. They are planned so as not to overlap with other events (for example communications windows) for power consumption.

The measurements of the magnetic sensor during one of the first activations in February 2006, are shown in Fig. 16. The first graph shows the magnitude of the components of the magnetic field in the satellite reference system and the variation of the modulus of the magnetic field. The satellite is precessing around the Z axis, the X and Y components being those that experiment a higher variation in magnitude during the spin.

The second graph shows the rotation of the magnetic field vector from the point of view of the satellite.

From this point the ACS must act on the attitude of the satellite to correct the spin.

Fig. 17 shows the magnetic field components measurements of two activations on September 25th and 26th, 2006. These activations correspond to passes in the vertical of Australia and South America, respectively, so as to contrast measurements in similar latitudes. The pictures in Fig. 17 show the position of NANOSAT-01 in the starting and ending points of each activation. These images were taken with Nova for Windows.

The components of the magnetic field in spherical coordinates from the reference system of the satellite are shown in Figs. 18, 19, and 20.

These are the real values needed by the ACS for the orientation of the satellite. From these graphics it can be seen that the satellite, in the moment of the activations, has no control of the attitude.

VII. CONCLUSIONS

Two years after the launch, the ACS magnetic sensor of NANOSAT 01 is correctly working to measure the magnetic field vector in the LEO, with a resolution of better that 0.1 mG.

As an experiment it can be said that the magnetic sensor COTS is likely to be space validated as it has been working properly during the first two years of the mission. Besides the communications by means of OWLS gives the sensor added value in versatility and autonomy. The optical wireless interface has also been reported to have been tested in flight with success [10].

As an essential part of the mission data of the magnetic field in the orbit with the resolution required for the attitude control of the satellite is being reported to the ACS.

In conclusion it can be said that the magnetic sensor is a success in the frame of the NANOSAT-01 mission, and this shows that AMR devices are a

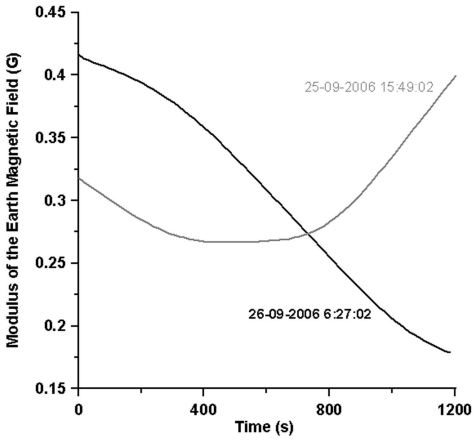

Fig. 18. Modulus of magnetic field in reference system satellite in two activations of September 2006: 25th at 15:49:02 UTC and 26th at 6:07:02 UTC.

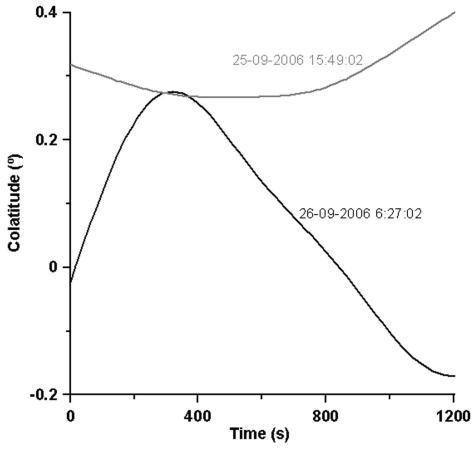

Fig. 19. Colatitude of magnetic field in reference system of satellite in two activations of September 2006: 25th at 15:49:02 UTC and 26th at 6:07:02 UTC.

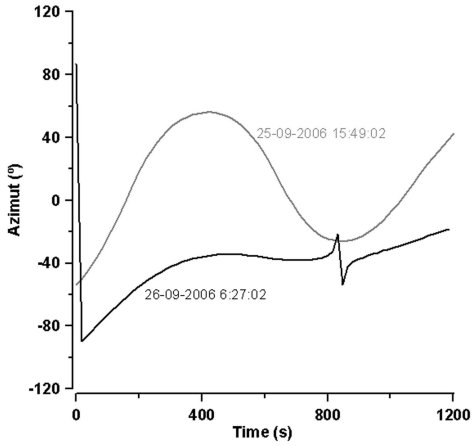

Fig. 20. Azimuth of magnetic field in reference system of satellite in two activations of September 2006: 25th at 15:49:02 UTC and 26th at 6:07:02 UTC.

good choice for space applications with medium to high requirements in sensitivity (≈ 3 mV/V/G) and resolution (≈ 30 μG), when the reduction of weight and mass are essential factors.

ACKNOWLEDGMENTS

The research in this paper was carried out by the Instituto Nacional de Técnica Aeroespacial—INTA. The authors wish to acknowledge R. P. del Real, G. Rosa, and A. Jiménez for the magnetic field simulator, J. J. Jiménez for support in the radiation tests, J. A. Fernández and E. Ragel for support in the up-screening process, and the NANOSAT-01 Team for its support.

REFERENCES

[1] Caceres, M.
The emerging nanosatellite market.
Aerospace America, **2** (2001), 16–18.

[2] Martinez, A., Arruego, I., Alvarez, M. T., Barbero, J., Guerrero, H., Levy, D., and Gras, A.
Nanosatellites technology demonstration.
In *Proceedings of the 14th AIAA/USU Conference on Small Satellites*, 2000.

[3] Nickel, J.
Magnetoresistance overview.
Hewlett-Packard Technical Report HPL-95-60 (06-1995).

[4] Caruso, M. J., and Bratland, T.
Anisotropic magnetoresistive sensors theory and applications.
Sensors Magazine, **16**, 3 (Mar. 1999), 18–26.

[5] 1- and 2-Axis Magnetic sensors HMC1001/1002, HMC1021/HMC1022 Datasheet. Available at www.ssec.honeywell.com/magnetic/datasheets/hmc 1001-28 1021-2.pdf.

[6] Jung, J., Kuzuya, N., and Alvarez, J.
The design of the OPAL attitude control system.
In *Proceedings of the 10th Annual AIAA/USU Small Satellite Conference*, 1996.

[7] Primdahl, F., Merayo, J. M. G., and Bauer, P.
In-flight spacecraft magnetic field monitoring using scalar/vector gradiometry.
Measurement Science and Technology, **17**, 2006.

[8] Janschek, K., Boge, T., Krasilshikov, M., Dishel, V., and Jacobson, M.
Minimum hardware navigation concept for LEO satellites using information fusion.
In *Proceedings of the 12th AIAA/USU Conference on Small Satellites*, 1998.

[9] Jimenez, J. J., Alvarez, M. T., Oter, J. M., Dominguez, J. A., Tamayo, R., Arruego, I., and Guerrero, H.
Proton radiation effects in medium/large area photodiodes and high power LED for optical wireless links for intra satellite communications (OWLS).
Presented at the Eighth European Conference on Radiation Effects on Components and Systems (RADECS 2005), Cap d'Adge, France, Sept. 19–23, 2005.

[10] Arruego, I., Martinez, J., Rodriguez, S., and Guerrero, H.
Optical wireless techniques demonstration on board nanosat-01.
Presented at the ESA Workshop on "Optical Wireless On-board Communications," ESA/ESTEC, Noordwijk, The Netherlands, Sept. 29–30, 2004.

Marina Díaz-Michelena received her M.Sc. (1998) in physical sciences at the Universidad Complutense de Madrid (UCM) and Ph.D. (2004) in applied physics at the Universidad Poletécnica de Madrid (UPM).

She is a researcher in magnetic sensors COTS (commercial off-the-shelf) based for Space applications at INTA, the Spanish National Institute of Aerospace Technology. She is an associate teacher in the Department of Physics of the Materials of the Faculty of Physics of UCM, and a collaborator in the evaluation of research and industrial projects of Xunta de Galicia, local government of Galicia, Spain.

Ignacio Arruego graduated as a Telecommunication Engineer in 1998 at the University of Zaragoza, Spain.

He worked as a H/W and EMC engineer at BOSCH-SIEMENS for 2 years, and joint INTA in 1999, where he works in the payloads area, within the Space Sciences Department. He has participed in several international R&D projects and in-orbit experiences, and contributed to more than 20 papers or international congresses. He also was a freelance collaborator of the spanish ANEP—Agencia Nacional de Evaluación y Prospectiva—during the year 2000, in several Technolgy-Watch activities.

Javier Martínez Oter received his Technical Engineer of Telecommunications (1999) and Electronic Engineer (2008) degrees from the Escuela Politécnica Superior de Alcalá de Henares.

He started working at the SAMe program, defined, developed, and produced the Standard Automatic Test System that will support all weapon systems in use with the Spanish Armed Forces and at the development of TPSs (Automatic test programs) for the F-18 plane. At present he works at the National Aerospace Institute of Spain (INTA), where he is a development engineer of all software and hardware for space missions. He works in the research of a platform technology for optical wireless intra-spacecraft communications. He has participated in the following projects: NANOSAT-1B, OPTOS, FOTON M3-OWLS, Optical Wireless Intra-Spacecraft Communications, OPTOMAG, Optical Wireless Layer Validation for on board data communications in an operational context, COTS optoelectronic for diffuse optical communications, NANOSAT, Demonstrator and optical communications modules by IR for the transmission of information Intra-Satellite.

Dr. Oter is author of seven publications.

Héctor Guerrero received his M.Sc. (1988) and Ph.D. (1992) in physical sciences from the Universidad Complutense de Madrid (UCM).

At present he is a researcher at the National Aerospace Institute of Spain (INTA), where he leads the Optoelectronics Laboratory. He is involved in the R&D of scientific payloads for space missions and of the development of a platform technology for optical wireless intra-spacecraft communications. In these activities he is the principal investigator in projects supported by the Spanish National Space Program and the European Space Agency. In relation to his university background, he was an associated lecturer at Universidad Complutense de Madrid in its Optics Department during the period 1988–1994 and as a part-time lecturer in 2001–2007. At a private university he was a lecturer of applied physics in 1994–1998. His research was related to physical optics, sensors, magneto-optics and optical fiber sensors.

Dr. Guerrero has coauthored more than 30 papers, 35 proceedings, and 5 patents in relation to applied physics (optoelectronics and magnetism) and space technology.